Citation for published version:
Thomas, B, Hunter, AJ & Dugelay, S 2020, 'Phase wrap error correction by random sample consensus with application to synthetic aperture sonar micro-navigation', *IEEE Journal of Oceanic Engineering*. https://doi.org/10.1109/JOE.2019.2960582

DOI:
10.1109/JOE.2019.2960582

Publication date:
2020

Document Version
Peer reviewed version

Link to publication

© 2020 IEEE. Personal use of this material is permitted. Permission from IEEE must be obtained for all other users, including reprinting/ republishing this material for advertising or promotional purposes, creating new collective works for resale or redistribution to servers or lists, or reuse of any copyrighted components of this work in other works.

University of Bath

Alternative formats
If you require this document in an alternative format, please contact:
openaccess@bath.ac.uk

General rights
Copyright and moral rights for the publications made accessible in the public portal are retained by the authors and/or other copyright owners and it is a condition of accessing publications that users recognise and abide by the legal requirements associated with these rights.

Take down policy
If you believe that this document breaches copyright please contact us providing details, and we will remove access to the work immediately and investigate your claim.

Download date: 05. May. 2023

Phase Wrap Error Correction by Random Sample Consensus with Application to Synthetic Aperture Sonar Micro-Navigation

Benjamin Thomas, *Student Member, IEEE,* Alan Hunter, *Senior Member, IEEE,* and Samantha Dugelay

Abstract

Accurate time delay estimation between signals is crucial for coherent imaging systems such as Synthetic Aperture Sonar (SAS) and Synthetic Aperture Radar (SAR). In such systems, time delay estimates resulting from the cross-correlation of complex signals are commonly used to generate navigation and scene height measurements. In the presence of noise, the time delay estimates can be ambiguous, containing errors corresponding to an integer number of phase wraps. These ambiguities cause navigation and bathymetry errors and reduce the quality of synthetic aperture imagery.

In this paper, an algorithm is introduced for detection and correction of phase wrap errors. The random sample consensus (RANSAC) algorithm is used to fit one- and two-dimensional models to the ambiguous time delay estimates made in the time delay estimation step of redundant phase centre (RPC) micro-navigation. Phase wrap errors are then corrected by re-calculating the phase wrap number using the best-fitting model.

The approach is demonstrated using data collected by the 270 - 330 kHz SAS of the NATO Centre for Maritime Research and Experimentation (CMRE) Minehunting Unmanned underwater vehicle for Shallow water Covert Littoral Expeditions (MUSCLE). Systems with lower fractional bandwidth were emulated by windowing the bandwidth of the signals to increase the occurrence of phase wrap errors. The time delay estimates were refined using both the RANSAC algorithms using one- and two- dimensional models and the commonly used branch-cuts method. Following qualitative assessment of the smoothness of the full-bandwidth time delay estimates after application of these three methods, the results from the 2D RANSAC method were chosen as the reference time delay estimates. Comparison with the reference estimates shows that the 1D and 2D RANSAC methods out-perform the branch-cuts method, with improvements of 29 - 125% and 30 - 150% respectively compared to 16 - 134% for the branch-cuts method for this dataset.

Index Terms

Time delay estimation, synthetic aperture sonar (SAS), synthetic aperture radar (SAR), phase unwrapping

Benjamin Thomas and Alan Hunter are with the University of Bath, UK

Samantha Dugelay is with the NATO Centre for Maritime Research and Experimentation, IT

Manuscript received Month Day, Year; revised Month Day, Year.

I. INTRODUCTION

Synthetic aperture radar (SAR) [1] and sonar (SAS) [2] are coherent imaging techniques that produce high resolution images of the Earth's surface above and below the water, respectively. Very precise estimation of time delays between coherent band-limited signals is essential for formation of a wide variety of SAS and SAR data products, including platform navigation solutions and 3D terrain maps.

It is known that the amplitude and phase of the cross-correlation function computed between complex band-limited coherent signals can be used to obtain a high precision estimate of the time delay between them [3], [4]. This high precision time delay estimate can be considered to be made up of a number of full phase wraps, plus a fraction of a phase wrap. In the presence of noise the estimate of the number of full phase wraps can be ambiguous [5]–[7], which is exacerbated for low fractional bandwidth signals. This ambiguity can corrupt the time delay estimate, reducing the accuracy of resulting data products such as through-the-sensor navigation algorithms [8], [9] or scene topography estimates [10], [11]. Therefore, detection and correction of phase wrap number errors is desirable.

Both SAS and SAR require sub-wavelength knowledge of the array path in order to support the coherent processing. While this can be achieved by radio navigation services such as GPS for satellite and airborne vehicles, underwater vehicles must make use of through-the-sensor micro-navigation techniques to achieve the required precision. Redundant phase centre (RPC) micro-navigation (also known as displaced phase centre antenna (DPCA) micro-navigation) [12]–[16] exploits high precision estimates of the time delay between signals received at overlapping sections of the virtual 'phase centre' array between successive pings. On each sonar ping, time delay estimates are computed between multiple pairs of time windowed signals, which results in time delay estimates as a function of ping number and range. An assumption of smoothness of this ensemble of estimates can be leveraged to identify and correct errors caused by phase wrapping.

There are existing methods of detecting phase wrap errors in RPC micro-navigation which exploit the assumption of smoothly varying time delay estimates as a function of range and ping number. By extension, this assumes a smoothly varying seafloor depth, and a smooth and continuous vehicle path. One method of removing outliers is to perform conventional phase unwrapping on the time delays from a single ping as a function of range only. This method achieves smoothly varying time delays, but is dependent on the seed used in the phase unwrapping and is not robust to the presence of gaps in the time delay estimate function. Path-following 2D unwrapping methods such as Goldstein's branch-cuts algorithm [17] have also been used [11]. However, such path-following phase unwrapping algorithms are unsuitable in applications where no unwrapping path exists with a maximum true change of phase per sample of π radians. This cannot guaranteed in all applications; in RPC micro-navigation this requirement is not met when the sway rate is larger than one wavelength per ping. A further approach uses model fitting to the time delay estimates in order to detect outliers. The random sample consensus (RANSAC) algorithm [18] has been proposed to achieve this [7], which is a popular method for model fitting in the presence of outliers. This method is more robust, but in this case only assumes smoothness of the time delay estimates in the range direction. A further method which exploits the smoothness of the time delay function in two dimensions has also been proposed

[6]. The method relies on finding regions of constant phase wrap number by detecting the location of phase wraps and discarding adjacent time delay estimates. The most commonly occurring phase wrap number estimate in each region is used to recalculate the time delays. This algorithm appears to give good performance. However it results in large amounts of data being discarded in applications where the phase gradient is large.

The problem of phase wrap error detection can be framed as a problem of robust regression in the presence of outliers, as demonstrated by [7]. Such problems occur frequently in the field of computer vision and numerous methods have been designed for solving them. These methods fall into three categories: M-estimators, case deletion diagnostics, and random sampling algorithms [19]. Despite the fact that methods with improved performance have been proposed [20]–[22], one of the most popular robust regression algorithms in computer vision is the random sample consensus (RANSAC) algorithm [18] due to its simplicity and high performance. Consequently we have chosen to use the RANSAC algorithm in this paper to detect phase wrap errors and identify error-free samples. The phase wrap errors are then corrected by re-unwrapping each estimate around the best-fitting model through the error-free samples.

The time delay estimation step of SAS RPC micro-navigation has been selected to demonstrate the method. We present field data collected by the CMRE MUSCLE AUV using its 270 - 330 kHz SAS during the MANEX14 experiment. In order to compare the method using 1D and 2D models, systems with a higher frequency-to-bandwidth ratio are emulated by artificially reducing the bandwidth of the sonar data before time delay estimation. This reduction in the bandwidth causes an increased number of phase wrap number estimation errors. The performance of the RANSAC methods with 1D and 2D models is assessed by comparing the resulting time delay estimates to those obtained from the full bandwidth data. The Goldstein branch-cuts method has been applied with the same region size as the 2D RANSAC method for comparison.

II. Time delay estimation between coherent signals

Estimation of the time delay between wide-sense stationary coherent signals can be achieved by finding the sub-sample peak of their cross-correlation function [11]. A two-step process is generally employed for complex signals where a coarse estimate is made by finding the peak of the cross-correlation function magnitude and then refined using the phase at the location of the coarse estimate [16].

Consider the complex cross-correlation function $\Gamma(t_n)$, where $t_n = n\Delta t$ is the time delay axis sampled at $n \in [0, N-1]$, where N is the number of time samples and Δt is the sample period. The location of the largest value of the cross-correlation magnitude provides the 'very coarse' time delay estimate, given by

$$\tau'' = \arg\max_n \{|\Gamma(t_n)|\}. \tag{1}$$

This is then refined by interpolation with a quadratic kernel. The analytical solution for the location of the peak of the parabola passing through the maximum value and its two adjacent samples is given by

$$\tau' = \frac{-0.5\left[|\Gamma(\tau''+\Delta t)| - |\Gamma(\tau''-\Delta t)|\right]}{|\Gamma(\tau''+\Delta t)| - 2|\Gamma(\tau'')| + |\Gamma(\tau''-\Delta t)|} \tag{2}$$

as derived in [23]. This provides the 'coarse' time delay estimate τ'.

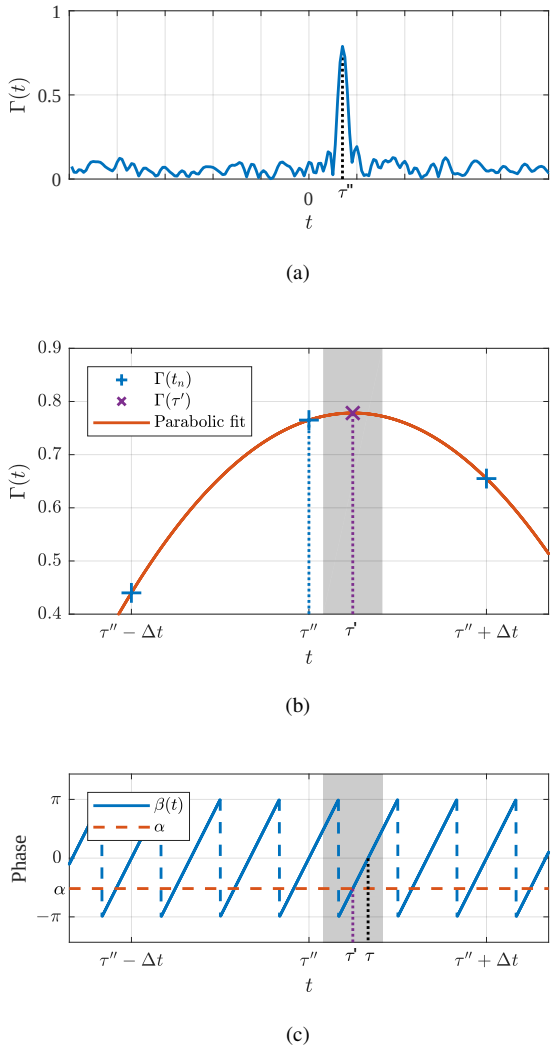

Fig. 1. Multi-stage time delay estimation. (a) A typical cross-correlation function, whose maximum at τ'' gives the very coarse time delay. (b) A parabola is fitted to peak of $\Gamma(t_n)$ and its adjacent samples. The peak of the parabola is the coarse time delay estimate τ'. (c) Candidate fine time delay estimates are shown at intersections of the modulated phase β with the measured phase α. The candidate closest to the parabola peak is chosen as the fine time delay estimate τ. The grey region has a width of one period at the centre frequency and is centred on τ', so the location of the only zero-crossing of the modulated phase function within this region gives the fine time delay estimate.

The 'fine' time delay estimate is given by

$$\tau = \left(-\frac{\alpha}{2\pi} + M\right)\frac{1}{f_c} \tag{3}$$

where

$$\alpha = \angle\Gamma(\tau'), \tag{4}$$

is the phase of the complex cross-correlation function linearly interpolated at τ' and $M \in \mathbb{Z}$ is the number of phase wraps, given by

$$M = \left\lfloor f_c\tau' + \frac{\alpha}{2\pi} \right\rceil, \tag{5}$$

where $\lfloor \dots \rceil$ denotes rounding to the nearest integer and f_c is the centre frequency of the signals.

Figure 1 depicts the time delay estimation process. Figure 1a shows a typical cross-correlation function, where the location of the maximum cross-correlation magnitude gives the very coarse time delay estimate τ''. The peak and its adjacent values are plotted in Figure 1b, through which a parabola is fitted. The location of the peak of this parabola gives the coarse time delay estimate τ', at which the phase of the cross-correlation function is interpolated, to give α. The underlying phase of the modulated cross-correlation function,

$$\beta(t) = \angle \exp\left(j\left(2\pi f_c\left(t-\tau\right)+\alpha\right)\right) \tag{6}$$

is assumed to be linear, as shown in Figure 1c. The correlation function at the carrier frequency is known to have zero phase at the true peak [11], and therefore candidate fine time delay estimates occur when the modulated phase of the cross correlation function crosses zero, i.e. when $\beta = 0$. The grey region centred on τ' has a width equal to the period at the centre frequency, such that the only candidate in this region is the fine time delay estimate τ. However, noise can cause a shift in the location of the cross-correlation peak τ', especially when the frequency-to-bandwidth ratio is high. This can result in an incorrect candidate fine time delay being chosen and thus errors in the phase wrap number estimate M.

The process described generates a single time delay estimate. In many applications, it is possible to repeat the process to produce multiple related time delay estimates. For example, the signals used in RPC micro-navigation are windowed in time, such that each windowed signal corresponds to a limited extent in range. Often, the related time delay estimates vary continuously and smoothly, reflecting an underlying continuous function. In these cases, this smoothness can be exploited to detect and correct phase wrap number errors.

III. Synthetic Aperture Sonar micro-navigation application

In SAS, sonar pings are transmitted towards the seafloor and their echoes are received as the vehicle travels along its path. These echoes are processed into an image by coherent summation along the synthetic aperture [2]. The speed of the vehicle and ping repetition frequency are chosen so that some array elements from subsequent pings overlap. The signals collected by the overlapping elements are coherent, and estimation of time delays between their signals forms the basis of RPC micro-navigation [16]. Figure 2a is a side view of the imaging geometry, where the vehicle is shown to travel close to the seafloor, with the sensor looking sideward and toward the seafloor. Inspecting the intersection of constant range arcs with the flat seafloor demonstrates a range-dependent difference in two-way range to a point on the seafloor due to the sway and heave of the sensor between pings. Figure 2b is a top view, showing the overlapping array elements between sonar pings. $\Delta\mathbf{x}_j$ represents the inter-ping displacement measured by RPC micro-navigation.

A. Redundant phase centre (RPC) algorithm

The first steps of the RPC micro-navigation algorithm involve finding the pairs of maximally overlapping array elements between subsequent pings, windowing their signals at multiple ranges, cross-correlating these windowed signals, and beam-steering the result over a range of angles. The cross-correlation function is then evaluated at the angle of maximum coherence [24]. Equations 1-5 can then used to estimate fine time delays.

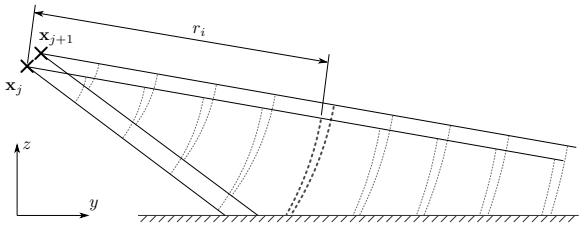

(a)

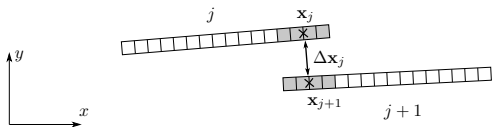

(b)

Fig. 2. (a) The side-looking geometry of RPC micro-navigation. $\mathbf{x}_j$ and $\mathbf{x}_{j+1}$ represent the RPC array positions for pings j and $j+1$ respectively. The straight lines represent the edges of the sonar beam, while dotted arcs represent lines of constant range from the sonar. Inspection of the intersection of these arcs with the flat seafloor reveals a range-dependent difference in two-way travel time difference due to inter-ping sway and heave (b) The side view of two arrays between pings, showing the overlapping phase centre array elements and the unknown displacement $\Delta\mathbf{x}_j$ to be measured by RPC micro-navigation.

Consider range windows indexed by the vector $i \in [0, I-1]$, where I is the number of range windows. Pings are indexed by $j \in [0, J-1]$, where J is the number of pings. The cross correlation function evaluated in the direction of maximum coherence at range window i and for the pair of pings j and $j+1$ is denoted $\Gamma_{i,j}(t_n)$, where n is the sample index. Fine time delays are estimated from each cross-correlation function using (3), resulting in the discrete two-dimensional function of fine time delay $\tau[i,j]$. Estimates with phase wrap number errors can be detected and corrected by exploiting the smoothness of this function.

B. Exploitation of seafloor continuity

In the SAS application, it is often reasonable to assume the seafloor is continuous and has a shape that changes smoothly. As a consequence, the time delays measured between signals received by overlapping array elements can be expected to change smoothly with range.

An example one-dimensional flat seafloor model has been used to demonstrate this, as illustrated in Figure 3. Let $\mathbf{x}_j = (y_j, z_j)^T$ and $\mathbf{x}_{j+1} = (y_{j+1}, z_{j+1})^T$ denote the positions of the RPC arrays for pings j and $j+1$ in the plane defined by the across-track y and vertical z directions. A point on the seafloor is denoted $\mathbf{x}_b = (y_b, z_b)^T$ and the inter-ping sway and heave are given by

$$\Delta y_j = y_{j+1} - y_j \tag{7}$$

and

$$\Delta z_j = z_{j+1} - z_j \tag{8}$$

respectively.

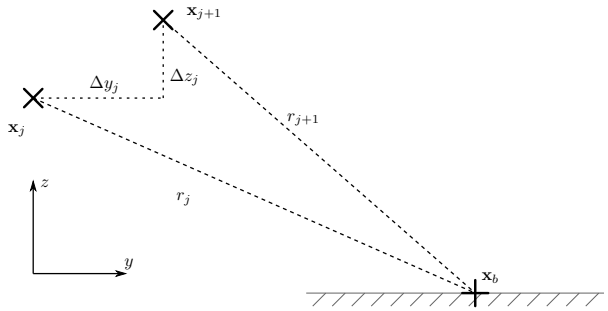

Fig. 3. The geometry for time delay estimation between signals collected by overlapping array elements in RPC micro-navigation, for a flat seafloor.

The one dimensional model for the time delay between the signals received by the overlapping arrays formed between ping j and $j+1$ is given by

$$\tau_{\text{flat}}(r) = \frac{2}{c}(r_{j+1} - r_j) \tag{9}$$

where c is the speed of sound in the medium,

$$r_j = \sqrt{(y_b - y_j)^2 + (z_b - z_j)^2} \tag{10}$$

is the distance between $\mathbf{x}_j$ and $\mathbf{x}_b$ and

$$r_{j+1} = \sqrt{(y_b - y_j - \Delta y_j)^2 + (z_b - z_j - \Delta z_j)^2} \tag{11}$$

is the distance between $\mathbf{x}_{j+1}$ and $\mathbf{x}_b$.

The resulting time delays as a function of range window for an example set of values for inter-ping sway and heave are shown in Figure 4, for a sensor altitude of $z_j = 12\,\text{m}$. The resulting time delays vary smoothly with range window due to the flat seafloor. Note that the smoothness of this function is contingent on a smooth seafloor; large, abrupt bathymetric features will cause discontinuities in the time delay as a function of range. Nevertheless, this model is representative of realistic time delay estimates between signals collected by the overlapping elements for a pair of pings during an experiment in the Ligurian sea, which are shown in Figure 5a. The majority of the experimental time delay estimates vary smoothly in the across-track direction, but some estimates are disparate from this trend by an integer number of time periods. Describing those disparate estimates as outliers and those that vary smoothly as inliers, the problem of detecting phase wrap errors may be framed as a robust regression problem in the presence of outliers. The random sample consensus (RANSAC) algorithm [18] is a popular method of solving such problems, and has been chosen for this application due to its remarkable combination of simplicity and high performance.

IV. Algorithm

In this section the algorithms used to perform phase wrap number error detection and correction are described. Firstly, a brief overview of the Random Sample and Consensus (RANSAC) [18] algorithm is given in IV-A. In

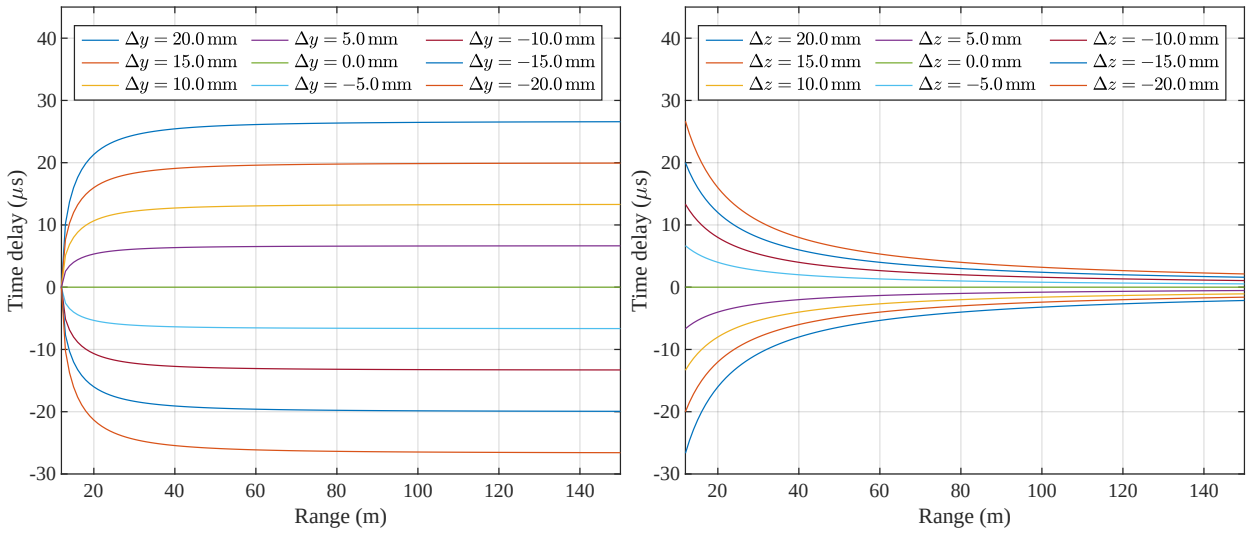

Fig. 4. Time delays caused by inter-ping (a) sway only, (b) heave only, for a sensor altitude of $z_j = 12\,\text{m}$.

Section IV-B, an overview of the method proposed in [7] is presented, which uses the RANSAC algorithm to fit a one-dimensional model to the time delay estimates as a function of range window. This model is used to detect and correct phase wrap number errors. The method is then developed and generalised in two salient ways described in Section IV-C: 1) the use of a two dimensional model in order to exploit the smoothness of the time delay estimates in a second dimension. 2) The size of the domain over which the model is fitted can be chosen in both dimensions, allowing the complexity of the model to be reduced while improving the resilience of the method to rapidly varying time delay estimates.

A. Random Sample and Consensus (RANSAC)

The RANSAC algorithm is a popular and robust method for detecting outliers, which is capable of finding a consensus set even when the ratio of outliers to samples is significant [18]. The algorithm repeatedly computes a model using a minimal data subset (i.e. the minimum number of samples required to fit the model), and finds the number of inliers for each candidate model. After a certain number of trials, the model with the largest number of inliers over all trials is deemed the optimal model.

The number of trials required to achieve a probability p of randomly drawing an all-inlier minimal subset can be adaptively computed on each iteration. It is given by [18]

$$K = \left\lceil \frac{\log_{10}(1-p)}{\log_{10}(1-\hat{w}^s)} \right\rceil, \tag{12}$$

where

$$\hat{w} = \frac{\hat{\eta}}{\Lambda} \tag{13}$$

is the largest estimate of the inlier ratio over all previous trials, where $\hat{\eta}$ is the largest number of inliers for all previous trials, Λ is the total number of data points and s is the number of samples in the minimal subset (i.e.

the number of parameters in the model). The required number of trials K is impacted heavily by the number of parameters in the chosen model when the inlier ratio is not close to 1, because the denominator of (12) approaches zero as $\hat{w}^s$ approaches zero. This motivates the use of a model with as few parameters as possible.

B. Phase wrap correction using a 1D continuity model

The use of a 1D model in the RANSAC error detection procedure exploits the expected smoothness of the time delay estimates as a function of range. The expected smoothness of the time delay estimates in the range direction was shown in Section III-B. In this work a quadratic model has been chosen to model the time delay estimates as a function of range. This choice is made without loss of generality due to the simplicity with which it can be computed and because it produces an acceptable fit to field data. An overview of the method applied to the time delays estimated between each pair of pings is given in Algorithm 1, and explained in more detail below with illustrations in Figure 5.

Consider fine time delay estimates $\tau_k[i]$, where $i \in [0, I-1]$ is the range index and I is the number of range windows. Additionally, let $k \in [0, K-1]$ denote the iteration number where K is the adaptively computed number of trials (12). Also let $\alpha_k[i]$ represent the phase measured at the cross-correlation function peaks.

On each iteration of the RANSAC algorithm, a quadratic model is fitted to a minimal data subset (3 samples in this case). The general form of the quadratic model for iteration k is given by

$$\widetilde{\tau}_k(r) = a_k r^2 + b_k r + c_k \tag{14}$$

where the coefficients a_k, b_k and c_k of the model that passes through the minimal data subset are computed by

$$\boldsymbol{a}_k = \boldsymbol{R}_k^{-1} \boldsymbol{\tau}_k \tag{15}$$

where

$$\boldsymbol{a}_k = \begin{pmatrix} a_k \\ b_k \\ c_k \end{pmatrix}, \tag{16}$$

is the vector containing the model coefficients,

$$\boldsymbol{R}_k = \begin{pmatrix} r^2[i_{1,k}] & r[i_{1,k}] & 1 \\ r^2[i_{2,k}] & r[i_{2,k}] & 1 \\ r^2[i_{3,k}] & r[i_{3,k}] & 1 \end{pmatrix} \tag{17}$$

is the matrix defining the polynomial model, and

$$\boldsymbol{\tau}_k = \begin{pmatrix} \tau[i_{1,k}] \\ \tau[i_{2,k}] \\ \tau[i_{3,k}] \end{pmatrix} \tag{18}$$

is the vector containing the minimal subset of time delay estimate samples, where $i_{1,k}$, $i_{2,k}$ and $i_{3,k}$ are randomly drawn without replacement from $i \in [0, I-1]$.

Algorithm 1 1D RANSAC

// Setup:

$k \leftarrow 0$ *// Initialise trial number*

$K \leftarrow \infty$ *// Initialise max. number of trials*

$\hat{\eta} \leftarrow 0$ *// Initialise number of inliers*

// Iterate:

while $k < K$ **do**

// Draw minimal data subset:

$i_{1,k} \sim \{x \in \mathcal{U}(0, I-1)\}$

$i_{2,k} \sim \{x \in \mathcal{U}(0, I-1) \,|\, x \notin i_{1,k}\}$

$i_{3,k} \sim \{x \in \mathcal{U}(0, I-1) \,|\, x \notin \{i_{1,k}, i_{2,k}\}\}$

// Calculate model coefficients:

$\boldsymbol{a}_k \leftarrow \boldsymbol{R}_k^{-1} \boldsymbol{\tau}_k$

// Calculate model time delays:

$\widetilde{\tau}_k(r) \leftarrow a_k r^2 + b_k r + c_k$

// Count number of inliers:

$\eta_k \leftarrow \sum_{i=0}^{I-1} \left[|\tau[i] - \widetilde{\tau}_k(r[i])| < t_{\text{thresh}} \right]$

// Test if model is better than previous best:

if $\eta_k > \hat{\eta}$ **then** *// Update*

$\hat{\eta} \leftarrow \eta_k$

$\hat{w} \leftarrow \eta_k / I$

$K \leftarrow \lceil \log_{10}(1-p) / \log_{10}(1-\hat{w}^s) \rceil$

$\kappa \leftarrow k$ *// Store trial number of best model*

end if

$k \leftarrow k + 1$ *// Increment trial number*

end while

// Re-calculate phase wrap numbers using model:

$\hat{M}[i] = \lfloor f_c \widetilde{\tau}_\kappa(r[i]) + \alpha[i]/2\pi \rceil$

// Re-calculate fine time delay estimates:

$\hat{\tau}[i] = \left(-\alpha[i]/2\pi + \hat{M}[i] \right) / f_c$

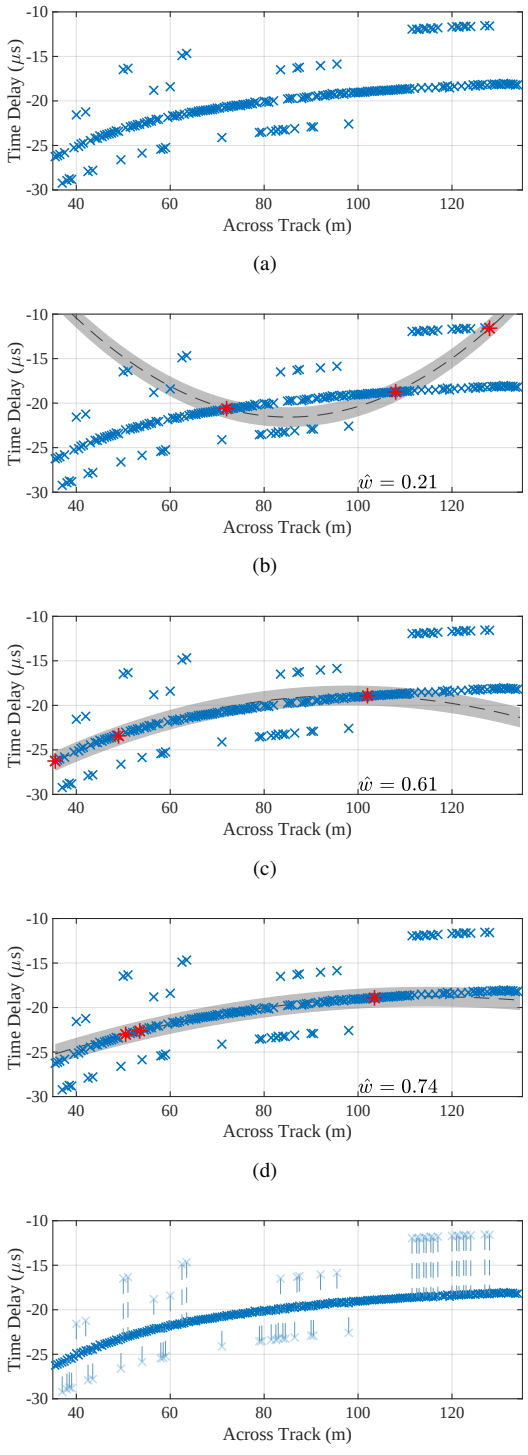

Fig. 5. Illustration of the 1D RANSAC algorithm using data from MANEX'14 (a) initial time delays shown by blue crosses, (b) a minimal subset shown by red crosses includes an outlier. The model shown by the black dashed line has few samples within the threshold shown by the grey region (c) all of a minimal subset are inliers but they define a sub-optimal model (d) another all-inlier minimal subset defines the optimal model (e) outliers are corrected, shown by blue dashed lines.

Having found the coefficients a_k, b_k and c_k, the model time delays at all ranges for trial k can be evaluated by substitution into (14), giving the model time delays $\widetilde{\tau}_k(r)$ for all ranges.

The number of samples considered to support the model, or 'inliers', is the total number of time delay estimates that lie within a predetermined threshold of the model. This number of samples that support the model is given by

$$\eta_k = \sum_{i=0}^{I-1} \Big[|\tau[i] - \widetilde{\tau}_k(r[i])| < \tau_{\text{thresh}} \Big] \tag{19}$$

where t_{thresh} is the threshold and $[\dots]$ denotes an Iverson bracket [25]. The value for τ_{thresh} must be chosen such that it is large enough to allow true variation of the time delays, but small enough for any estimates with phase wrap number errors to be rejected. In this work, a value of

$$\tau_{\text{thresh}} = \frac{1}{3f_c} \tag{20}$$

has been chosen, which corresponds to one third of a time period for the centre frequency.

For every iteration, if η_k is greater than the previous largest number of inliers $\hat{\eta}$, the best estimate of the inlier fraction and the required number of trials are updated using (13) and (12) respectively.

An example of a minimal subset of three samples including two inliers and one outlier is shown in Figure 5b. The grey band represents the region in which samples are considered to be inliers, i.e. they are within the predetermined threshold of the model. For this particular minimal subset of 3 data points, the quadratic model has very poor support. In Figure 5c an all-inlier minimal subset with poor coverage has been selected. In this case, the model has greater support, but the model selected in Figure 5d has even better support and is eventually chosen as the optimal model.

The process is iterated until the adaptively computed number of trials K has been performed, at which point a subset of time delay estimates have been identified as outliers. Figure 5e shows the correction of the outliers by adjusting the phase wrap number as follows.

The updated phase wrap number is given by

$$\hat{M}[i] = \left\lfloor f_c \widetilde{\tau}_\kappa(r[i]) + \frac{\alpha[i]}{2\pi} \right\rceil, \tag{21}$$

and the resulting refined time delay estimate calculated by

$$\hat{\tau}[i] = \left(-\frac{\alpha[i]}{2\pi} + \hat{M}[i] \right) \frac{1}{f_c} \tag{22}$$

is retained if

$$|\hat{\tau}[i] - \widetilde{\tau}_\kappa(r[i])| < \tau_{\text{thresh}} \tag{23}$$

and discarded otherwise. In Figure 5e, all of the outliers were corrected, with none being discarded.

C. Phase wrap correction using a 2D model

A 2D model can be used to exploit the expected smoothness of time delay estimates in two dimensions (e.g. ping number and range). A 2D sliding rectangular window is used to extract regions of the time delay estimates

Algorithm 2 2D RANSAC

// Setup:

$k \leftarrow 0$ *// Initialise trial number*

$K \leftarrow \infty$ *// Initialise max. number of trials*

$\hat{\eta} \leftarrow 0$ *// Initialise number of inliers*

// Iterate:

while $k < K$ **do**

// Draw minimal data subset:

$i_{1,k} \sim \{x \in \mathcal{U}(0, I-1)\}$

$j_{1,k} \sim \{x \in \mathcal{U}(0, J-1)\}$

$i_{2,k} \sim \{x \in \mathcal{U}(0, I-1) \,|\, x \notin i_{1,k}\}$

$j_{2,k} \sim \{x \in \mathcal{U}(0, J-1) \,|\, x \notin j_{1,k}\}$

$i_{3,k} \sim \{x \in \mathcal{U}(0, I-1) \,|\, x \notin \{i_{1,k}, i_{2,k}\}\}$

$i_{3,k} \sim \{x \in \mathcal{U}(0, J-1) \,|\, x \notin \{j_{1,k}, j_{2,k}\}\}$

$i_{4,k} \sim \{x \in \mathcal{U}(0, I-1) \,|\, x \notin \{i_{1,k}, i_{2,k}, i_{3,k}\}\}$

$i_{4,k} \sim \{x \in \mathcal{U}(0, J-1) \,|\, x \notin \{j_{1,k}, j_{2,k}, j_{3,k}\}\}$

// Calculate model coefficients:

$\boldsymbol{a}_k \leftarrow \boldsymbol{R}_k^{-1} \boldsymbol{\tau}_k$

// Calculate model time delays:

$\widetilde{\tau}_k(r, u) = a_k r + b_k u + c_k u^2 + d_k$

// Count number of inliers:

$\hat{\eta}_k = \sum_{i=0}^{I-1} \sum_{j=0}^{J-1} \left[|\tau[i,j] - \widetilde{\tau}_k(r[i], u[j])| < \tau_{\text{thresh}} \right]$

// Test if model is better than previous best:

if $\eta_k > \hat{\eta}$ **then** *// Update*

$\hat{\eta} \leftarrow \eta_k$

$\hat{w} \leftarrow \eta_k / IJ$

$K \leftarrow \lceil \log_{10}(1-p) / \log_{10}(1-\hat{w}^s) \rceil$

$\kappa \leftarrow k$ *// Store trial number of best model*

end if

$k \leftarrow k + 1$ *// Increment trial number*

end while

// Re-calculate phase wrap numbers using model:

$\hat{M}[i,j] = \lfloor f_c \widetilde{\tau}_\kappa(r[i,j]) + \alpha[i,j]/2\pi \rceil$

// Re-calculate fine time delay estimates:

$\hat{\tau}[i,j] = \left(-\alpha[i,j]/2\pi + \hat{M}[i,j] \right) / f_c$

over which a model is fitted. The choice of model and window size are application dependent but must be chosen such that the windowed time delay estimates can be adequately represented by the chosen model.

The RANSAC algorithm is applied to each 2D window in turn. Outliers are detected by iteratively fitting a 2D model to a minimal data subset of the windowed time delay estimates, and finding the model with the largest number of inliers. The refined time delay estimates are then calculated using the best model. Duplicate refined time delay estimates can be generated if overlapping 2D windows are used. The mode of any duplicates is taken once refined time delay estimates have been made for all 2D windows. The algorithm for each 2D window is summarised in Algorithm 2.

The RPC micro-navigation algorithm computes time delay estimates at multiple ranges and multiple ping pairs along the vehicle's path. This 2D function can be assumed to be smooth in both dimensions by virtue of the continuous seafloor in combination with the vehicle's inertia. Consider the fine time delay estimates $\tau[i, j]$, which represent a rectangularly windowed region of time delays indexed by $i \in [0, I-1]$ and $j \in [0, J-1]$, where I is the number of range windows and J is the number of pings. Also let $\alpha[i, j]$ represent the measurements of the phase at the peak of the cross-correlation function over the same region.

The RANSAC algorithm iteratively selects a minimal subset of time delay estimates at random and computes the parameters of a model. The model must be selected carefully to suit the application. In this application, a model of the form

$$\widetilde{\tau}_k(r, u) = a_k r + b_k u + c_k u^2 + d_k \tag{24}$$

is used on each iteration $k \in [0, K-1]$, which is quadratic in the along-track direction and linear in the range direction. This model has been chosen in this application because the gradient of the time delay estimates varies more rapidly in the along-track direction than in the range direction in field data due to the AUV motion, as can be observed in Figure 9a.

For each trial k, the coefficients a_k b_k, c_k and d_k are computed by

$$\boldsymbol{a}_k = \boldsymbol{R}_k^{-1} \boldsymbol{\tau}_k, \tag{25}$$

where

$$\boldsymbol{a}_k = \begin{pmatrix} a_k \\ b_k \\ c_k \\ d_k \end{pmatrix}, \tag{26}$$

is the vector containing the model coefficients,

$$\boldsymbol{R}_k = \begin{pmatrix} r[i_{1,k}] & u[j_{1,k}] & u[j_{1,k}]^2 & 1 \\ r[i_{2,k}] & u[j_{2,k}] & u[j_{2,k}]^2 & 1 \\ r[i_{3,k}] & u[j_{3,k}] & u[j_{3,k}]^2 & 1 \\ r[i_{4,k}] & u[j_{4,k}] & u[j_{4,k}]^2 & 1 \end{pmatrix} \tag{27}$$

is the matrix defining the model, and

$$\boldsymbol{\tau}_k = \begin{pmatrix} \tau_k[i_{1,k}, j_{1,k}] \\ \tau_k[i_{2,k}, j_{2,k}] \\ \tau_k[i_{3,k}, j_{3,k}] \\ \tau_k[i_{4,k}, j_{4,k}] \end{pmatrix} \tag{28}$$

is the vector containing the minimal subset of time delay estimate samples, where $i_{1,k}, ..., i_{4,k}$ and $j_{1,k}, ..., j_{4,k}$ are drawn without replacement from $i \in [0, I-1]$ and $j \in [0, J-1]$ respectively.

Similarly to the 1D RANSAC algorithm, the model time delays can be evaluated at all ranges by substitution into (24), giving the model time delays $\widetilde{\tau}_k(r, u)$. The number of samples that support the model (or inliers) is given by

$$\hat{\eta}_k = \sum_{i=0}^{I-1} \sum_{j=0}^{J-1} \left[|\tau[i,j] - \widetilde{\tau}_k(r[i], u[j])| < \tau_{\text{thresh}} \right] \tag{29}$$

where τ_{thresh} is the threshold and $[\dots]$ denotes an Iverson bracket. If the model has more support than the previous best number of inliers, the number of trials is updated using (12), where the new best estimate of the inlier fraction is given by

$$\hat{w} = \frac{\hat{\eta}}{IJ}. \tag{30}$$

Once K trials have been completed, a subset of time delay estimates are identified as outliers. The following phase wrap number correction can be applied to all time delay estimates, since inliers are unchanged by the correction.

The updated phase wrap number is given by

$$\hat{M}[i,j] = \left\lfloor f_c \widetilde{\tau}_\kappa[i,j] + \frac{\alpha[i,j]}{2\pi} \right\rceil, \tag{31}$$

and the resulting refined time delay estimate calculated by

$$\hat{\tau}[i,j] = \left(-\frac{\alpha[i,j]}{2\pi} + \hat{M}[i,j] \right) \frac{1}{f_c} \tag{32}$$

is retained if

$$|\hat{\tau}\left[i,j\right] - \widetilde{\tau}\left(r\left[i\right], u\left[j\right]\right)| < \tau_{\text{thresh}} \tag{33}$$

and discarded otherwise. Again, the threshold chosen in this work is given by (20).

The algorithm is demonstrated for one particular windowed subset of time delays in Figure 6. The initial fine time delay estimates $\tau[i,j]$ are shown in Figure 6a, which shows the majority of the time delay estimates vary smoothly in both the ping axis and the across track axis, with some outliers present. Figure 6b shows a minimal subset that includes outliers. The grey surfaces represent the upper and lower limits of the region in which the time delay estimates are considered inliers. Figure 6c shows an iteration where all of the minimal data subset are inliers, which results in a model with the largest support. Once the required number of trials has been performed, the outliers are corrected by adjusting the phase wrap number, the result of which is shown in Figure 6d. In this case, no time delay estimates were discarded.

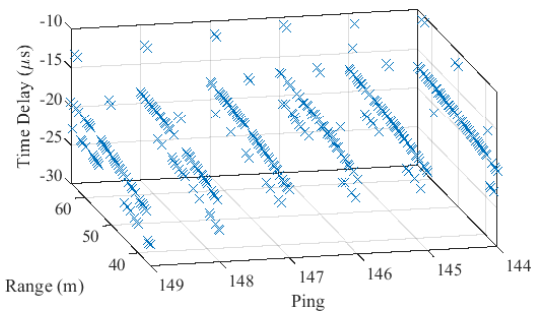

(a)

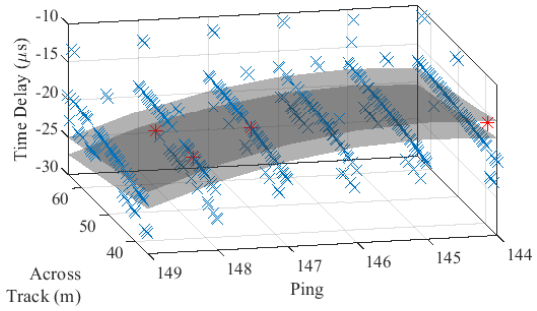

(b)

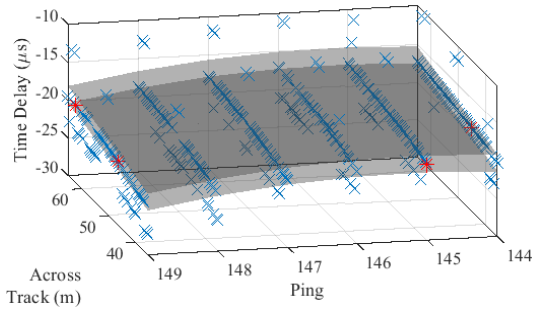

(c)

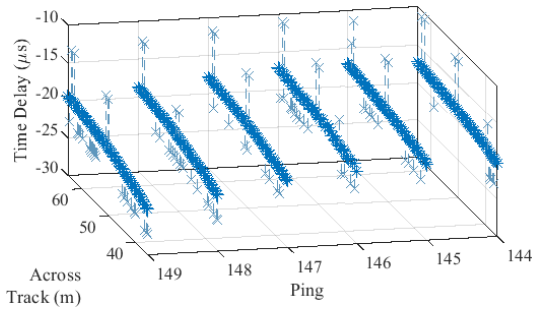

(d)

Fig. 6. Illustration of the 2D RANSAC algorithm using data from MANEX'14 (a) initial time delay estimates, shown by blue crosses (b) a minimal subset shown by red crosses includes an outlier, so the model has poor support. The grey surfaces are the upper and lower thresholds (c) the minimal subset is contains only inliers, and has good support (d) the blue dashed lines show the outliers being corrected using the optimal model.

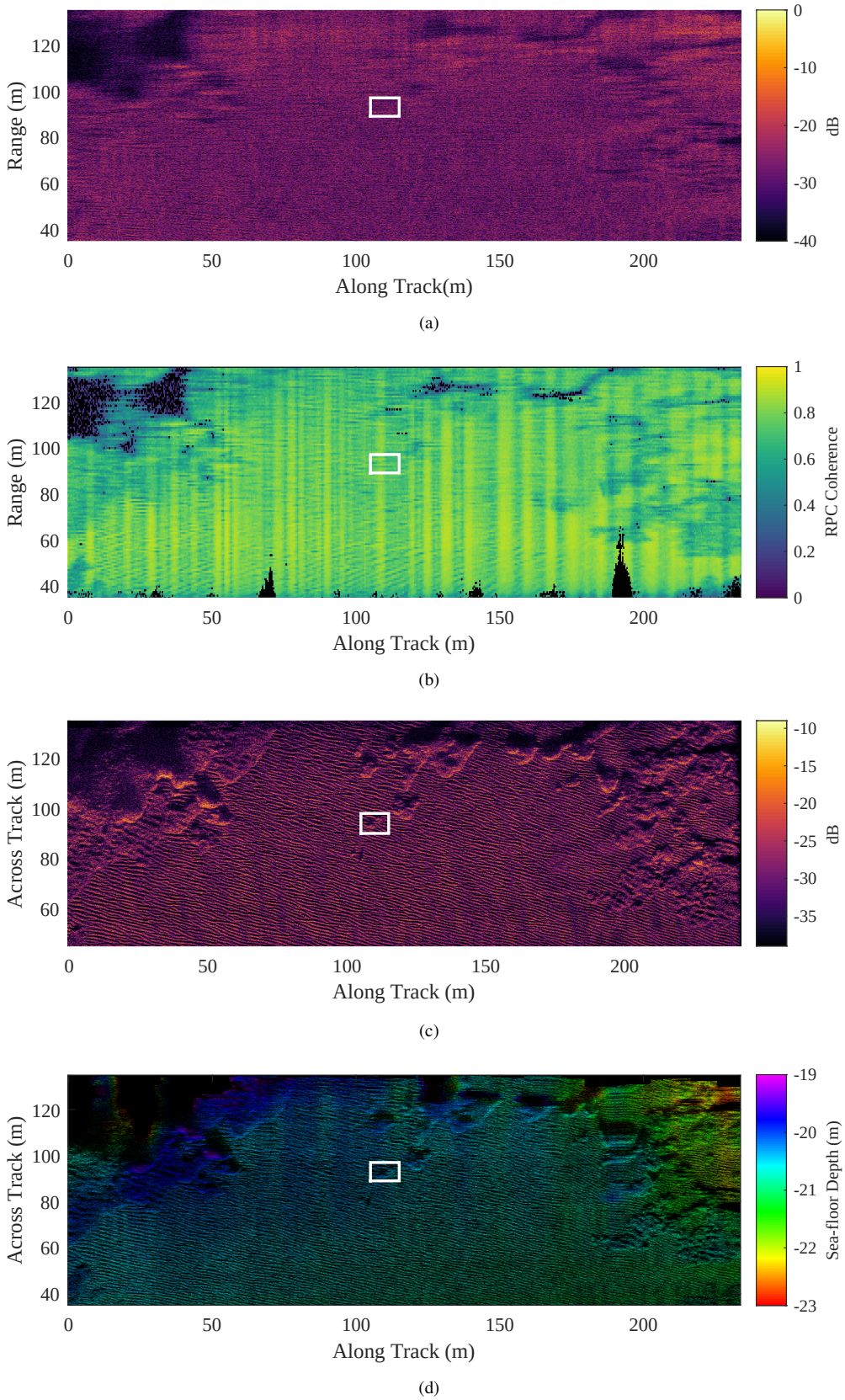

Fig. 7. (a) Sonar echo data. (b) RPC coherence. (c) SAS image showing a predominantly rippled, sandy seafloor. (d) Bathymetry generated by sidescan interferometry without motion compensation. A small sub-window has been chosen to show the effect of reducing the frequency bandwidth of the data.

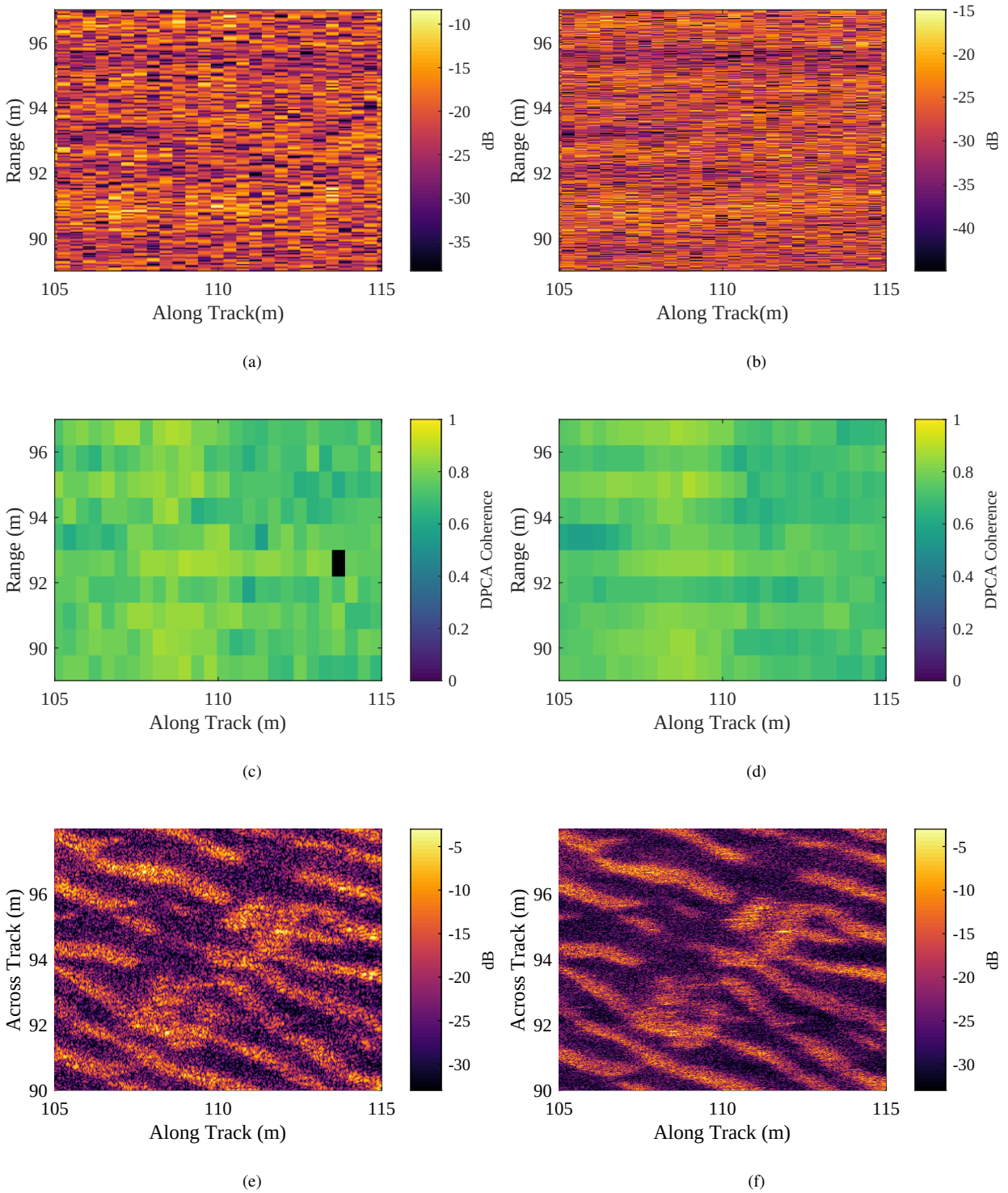

Fig. 8. Zoom of (a,b) raw data, (c,d) coherence, (e,f) SAS images. Left column (a,c,e) 10 kHz bandwidth. Right column (b,d,f) 60 kHz bandwidth.

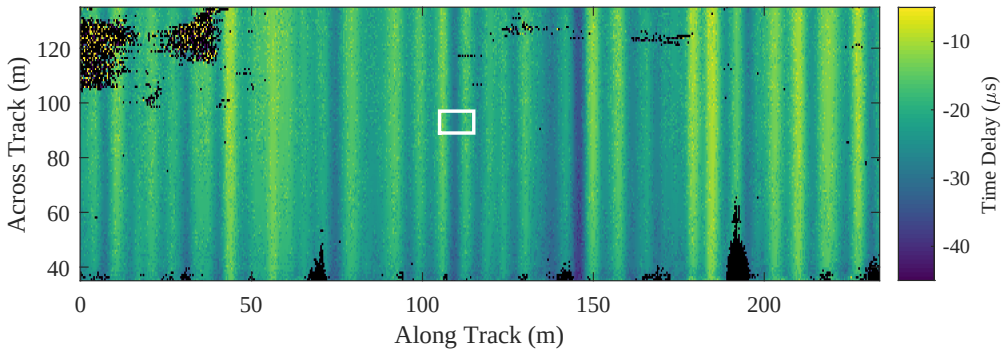

(a)

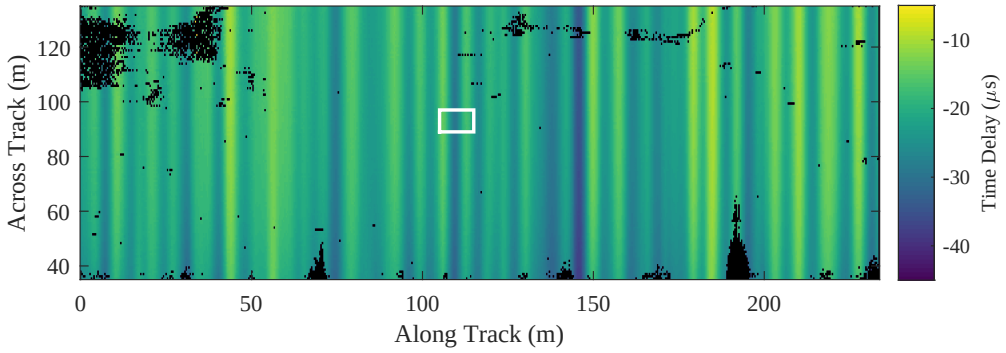

(b)

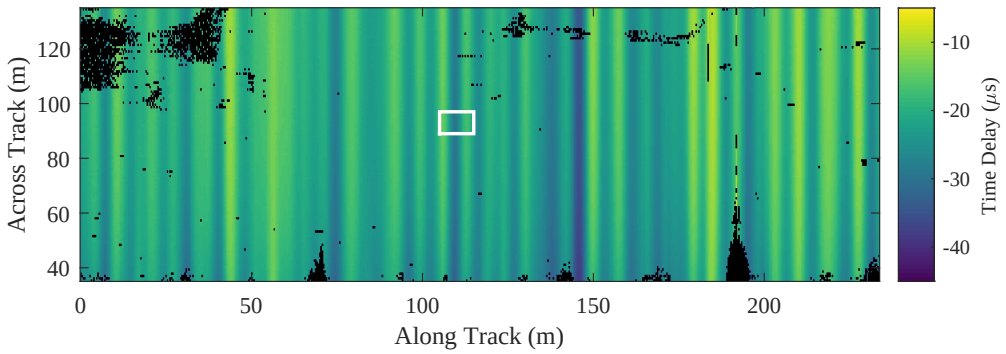

(c)

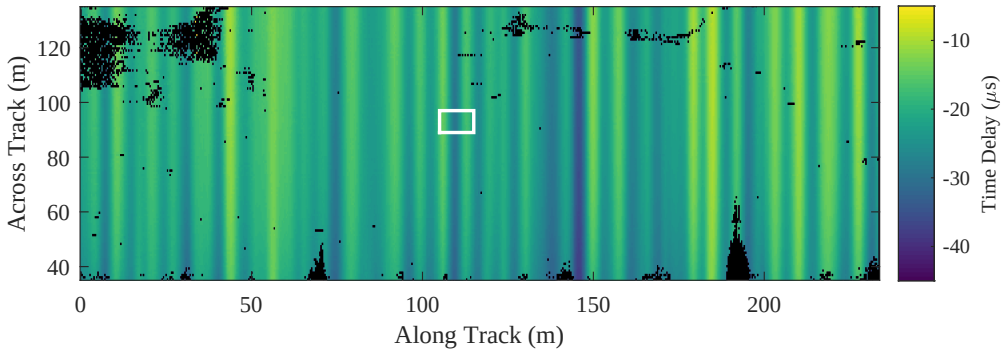

(d)

Fig. 9. (a) Time delays from 60 kHz bandwidth data. (b) Refined time delays using the branch-cuts method. (c) Refined time delays using the 1D RANSAC method. (d) Refined time delays using the 2D RANSAC method.

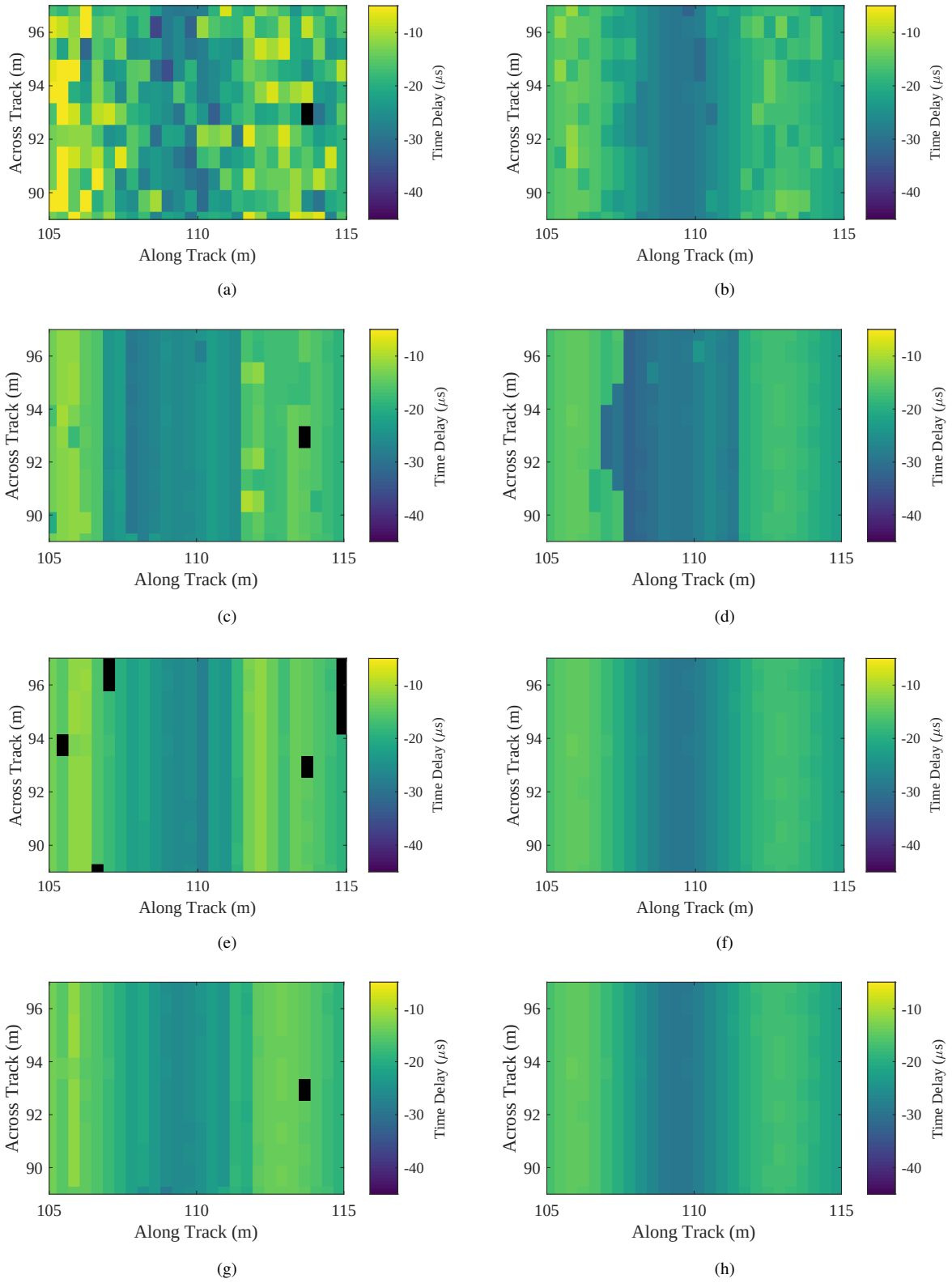

Fig. 10. Zooms of: (a,b) Unrefined time delays. (c,d) Refined time delays using the branch-cuts method. (e,f) Refined time delays using the 1D RANSAC method. (g,h) Refined time delays using the 2D RANSAC method. Left column (a,c,d,g) 10 kHz bandwidth. Right Column (b,d,f,h) 60 kHz bandwidth.

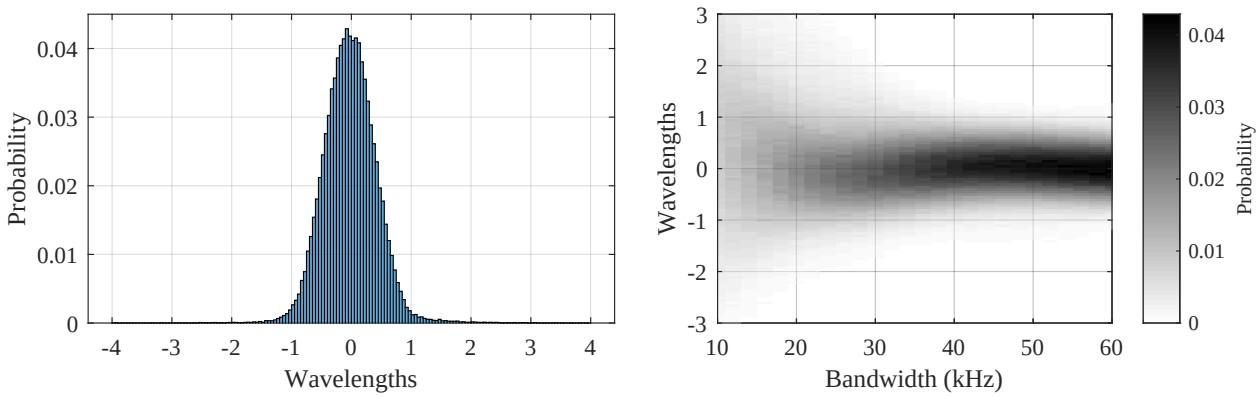

(a) (b)

Fig. 11. (a) Probability distribution of error between coarse time delay estimates from 60 kHz bandwidth around the gold standard fine time delay estimates. (b) The probability distribution of the coarse time delay error as a function of bandwidth.

V. Experimental Method and Results

SAS data were collected by the CMRE MUSCLE platform over a frequency range of 270 - 330 kHz during the MANEX'14 sea trial. The vehicle was programmed to perform a straight track at a constant altitude of 12 m above the seafloor. The unprocessed SAS echo data collected on a particular track are shown in Figure 7a. The inter-ping coherence is shown in Figure 7b. The resulting SAS image is shown in Figure 7c, which reveals a predominantly sandy, rippled seafloor, with some rocks and posidonia. The vehicle was not running in interferometric mode and therefore it is not possible to generate a bathymetry map using SAS interferometry [26]. However, sidescan interferometry can be used to produce a low-resolution depth map, which is shown in Figure 7d. A small subset of the echo data, coherence and SAS images have been selected for closer inspection, which are marked by white rectangles in Figure 7.

The frequency bandwidth of the data has been windowed to between 60 kHz and 10 kHz using a Tukey window [27] with 10% transition width. This emulates systems with lower fractional bandwidth, demonstrating the effect of reducing the frequency bandwidth of the data. The subsets of the echo data, coherence and SAS image for frequency bandwidths of 10 kHz and 60 kHz are shown in Figure 8. A reduction in across-track resolution is evident in Figures 8a and 8e (10 kHz bandwidth) when compared with Figures 8b and 8f (60 kHz bandwidth), as expected since the across-track resolution is proportional to the inverse of the bandwidth [28]. The values of the coherence estimates are similar between Figures 8c and 8d (with mean values of 0.75 and 0.73 for 10 kHz and 60 kHz respectively). The variances of the coherence estimates are 3.5×10^{-3} and 3.8×10^{-3} at 10 kHz and 60 kHz respectively.

The time delays estimated from the full-bandwidth (60 kHz) data are shown in Figure 9a. Subsets of the time delays estimated using the 10 kHz and 60 kHz bandwidth data are shown in Figures 10a and 10b respectively. Black regions represent samples where no time delay estimate was made due to low coherence magnitude. A coherence threshold of 0.3 is used, which corresponds to a value three standard deviations larger than the expected coherence value for random signals of the length of the range windows. What appear to be randomly distributed phase wrap

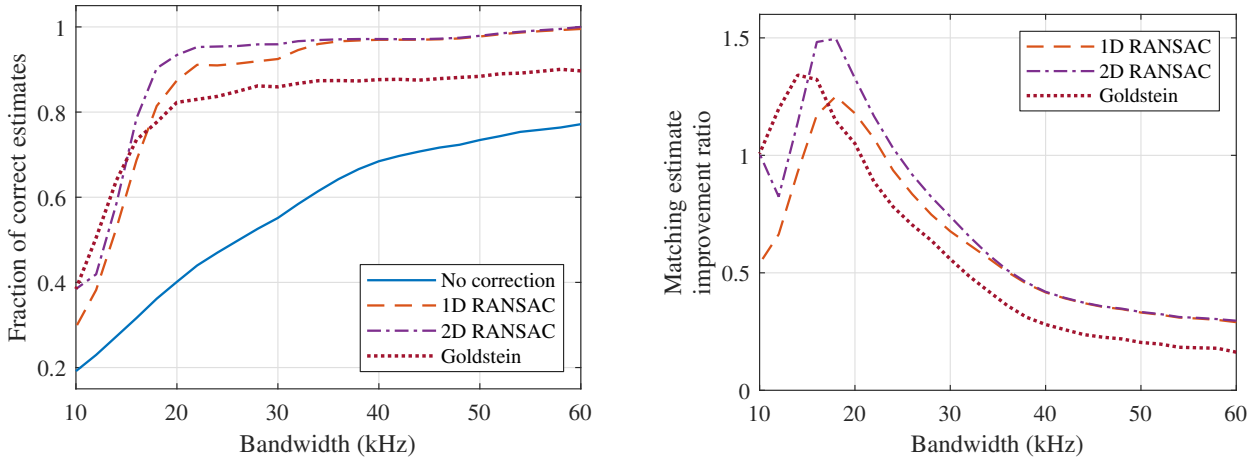

(a) (b)

Fig. 12. (a) Fraction of time delay estimates that match the reference with no correction, after 1D and 2D RANSAC methods, and using the branch-cuts method (b) The matching estimate improvement ratios for each of the methods.

number errors are visible, and are much more prevalent in the 10 kHz data (Figures 10a) than the 60 kHz data (Figure 10b) as expected.

The 1D and 2D RANSAC methods have been applied to the time delays measured using the frequency band-limited data. The branch-cuts method has also been applied over the same window sizes as the 2D RANSAC method for comparison. The resulting refined time delay estimates for the 60 kHz data using the 1D and 2D RANSAC methods are shown in Figures 9c and 9d respectively. The result from the branch-cuts method is shown in Figure 9b. Subsets of the refined time delays estimated using the 10 kHz and 60 kHz bandwidth data are shown in Figures 10e and 10f for the 1D RANSAC method, Figures 10g and 10h for the 2D RANSAC method, and Figures 10c and 10d for the branch-cuts method.

At 60 kHz bandwidth, the 1D and 2D RANSAC methods generate extremely similar estimates. However, the branch-cuts method shows discontinuities in the along-track direction (shown in Figure 9b), which correspond to regions of large ($> \pi$) phase differences caused by large inter-ping sways. At 10 kHz bandwidth, some time delay estimates refined using the 1D and 2D RANSAC methods have been rejected due to being further than the threshold from the model, which are shown as black regions in Figures 10e and 10g.

The time delays estimated using the bandwidth-filtered data are denoted by $\hat{\tau}_{b,\mathrm{R1}}[i,j]$, $\hat{\tau}_{b,\mathrm{R2}}[i,j]$ and $\hat{\tau}_{b,\mathrm{GS}}[i,j]$ for the 1D and 2D RANSAC methods and the branch-cuts algorithm respectively, where $b \in \{10, 12, 14, ..., 60\}$ kHz indexes the frequency bandwidths.

The results from the 1D RANSAC, 2D RANSAC and branch-cuts methods at full frequency bandwidth were qualitatively assessed based on the smoothness of the resulting time delay estimates, and the 2D RANSAC method was found to give the best results. The time delay estimates from the 2D RANSAC algorithm, denoted $\hat{\tau}_{B,\mathrm{2D}}[i,j]$, are therefore considered to be the 'gold standard' time delay estimates in the following analysis.

The probability distribution of the error in the coarse time delay estimates (compared to the gold standard time

delay estimates) is shown in Figure 11. The error distribution at full 60 kHz bandwidth is shown in Figure 11a, which is symmetrical and centred on zero error as expected. However, this clearly illustrates the problem that must be solved; the fine time delay estimation procedure described in Section II gives inaccurate estimates for coarse time delay estimates with an error corresponding to more than half a wavelength. Figure 11b is the error distribution with varying bandwidth, which shows a broadening of the error distributions with reducing bandwidth. A slight asymmetry is also evident at smaller bandwidths, possibly caused by the assumption of zero relative dilation between signals which may be inaccurate at short range.

The refined time delay estimates from the 1D and 2D RANSAC methods and the branch-cuts method at each frequency bandwidth have been compared with the gold standard time delay estimates. The fraction of the time delay estimates that match the gold standard is given by

$$\xi_{b,\mu} = \frac{\sum_{i=0}^{I-1}\sum_{j=0}^{J-1}\Big[\,|\hat{\tau}_{b,\mu}[i,j] - \hat{\tau}_{B,\text{2D}}[i,j]| < \tau_{\text{thresh}}\Big]}{IJ} \tag{34}$$

where μ denotes the correction method.

The resulting values of $\xi_{b,\mu}$ are plotted in Figure 12a. The matching estimate improvement ratios calculated by

$$\zeta_{b,\mu} = \frac{\xi_{b,\mu} - \xi_{b,\text{NC}}}{\xi_{b,\text{NC}}} \tag{35}$$

are plotted in Figure 12b. This demonstrates that the 1D and 2D RANSAC methods result in what we interpret as improvements of 29 - 125% and 30 - 150% respectively compared to 16 - 134% for the Goldstein branch-cuts method.

The ratio of matching estimates for the unrefined time delay estimates reduces with decreasing bandwidth, because the width of the peak of the correlation function becomes wider with decreasing frequency bandwidth. This broadening of the cross-correlation peak means that noise is more likely to cause phase wrap errors. The 1D and 2D RANSAC methods perform at least as well as the branch-cuts method at all frequency bandwidths. The branch-cuts method performs less well than the RANSAC methods at high bandwidths due to its inability to unwrap regions with high phase gradient correctly.

The time taken to perform the methods at each bandwidth is plotted in Figure 13. With reducing bandwidth, the time taken for both RANSAC methods increases due to the reducing inlier fraction, which causes the number of RANSAC iterations to increase. However, this is particularly evident for the 2D RANSAC method, because the number of parameters in the model is larger, meaning more trials are required to achieve the same probability of success. The time taken by the branch-cuts method is approximately constant for all frequency bandwidths.

VI. Conclusion and Further Work

Algorithms making use of the RANSAC algorithm with 1D and 2D models have been developed to detect and correct phase wrap number errors in time delay estimation applications. Results from field data collected by the 270 - 300 kHz SAS of the CMRE MUSCLE AUV show that the 1D and 2D RANSAC methods result in improvements of 29 - 125% and 30 - 150% respectively compared to improvements of 16 - 134% for the Goldstein branch-cuts

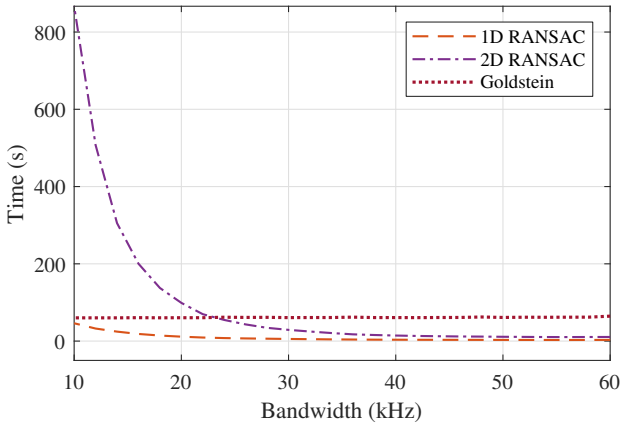

Fig. 13. Time taken by the 1D RANSAC, 2D RANSAC and Goldstein branch cuts methods.

method. Using a 2D model shows a slight performance benefit, at the expense of greater computational cost than using a 1D model. These model-based approaches to the phase unwrapping problem have been shown to be resilient to regions of high phase gradient, which result in errors for the branch-cuts method.

Application of these algorithms to RPC micro-navigation will increase the accuracy of through-the-sensor navigation estimation and is therefore likely to improve SAS image quality. The algorithms have been shown to be effective for a large range of bandwidths, which may enable the use of lower cost, low fractional bandwidth systems. Repeat-pass SAS has the potential to generate very high precision 3D seabed maps, and application of these algorithms provides the high accuracy time delay estimates required for repeat-pass micro-navigation algorithms.

ACKNOWLEDGEMENT

The authors would like to thank the scientists and engineers in the Autonomous Mine Countermeasures team at the NATO Science and Technology Organisation (STO) Centre for Maritime Research and Experimentation (CMRE) and the crew of the NRV Alliance for their support during the MANEX14 sea trial. They are also grateful to CMRE and the UK Defence Science and Technology Laboratory (Dstl) for supplying the trial data. CMRE are funded by the NATO Allied Command Transformation. B. W. Thomas thanks CMRE for hosting him during summer 2017, and both the James Dyson Foundation and the US Office of Naval Research (Grant No. N00014-19-1-2452) for funding his research.

REFERENCES

[1] A. Moreira, P. Prats-Iraola, M. Younis, G. Krieger, I. Hajnsek, and K. P. Papathanassiou, "A tutorial on synthetic aperture radar," *IEEE Geoscience and Remote Sensing Magazine*, vol. 1, no. 1, pp. 6–43, Mar 2013.

[2] M. P. Hayes and P. T. Gough, "Synthetic Aperture Sonar: A Review of Current Status," *IEEE Journal of Oceanic Engineering*, vol. 34, no. 3, pp. 207–224, Jul 2009.

[3] G. Carter, "Time delay estimation for passive sonar signal processing," *IEEE Transactions on Acoustics, Speech, and Signal Processing*, vol. 29, no. 3, pp. 463–470, Jun 1981.

[4] A. H. Quazi, "An overview of time delay estimation in active and passive system for target localization," *IEEE Transactions on Acoustics, Speech, and Signal Processing*, vol. ASSP-29, no. 3, pp. 527–533 ST – An overview of time delay estimation, 1981.

[5] T. O. Sæbø, R. E. Hansen, and A. Hanssen, "Relative height estimation by cross-correlating ground-range synthetic aperture sonar images," *IEEE Journal of Oceanic Engineering*, vol. 32, no. 4, pp. 971–982, 2007.

[6] S. Leier, "Signal Processing Techniques for Seafloor Ground-Range Imaging Using Synthetic Aperture Sonar Systems," PhD Thesis, Technische Universität Darmstadt, 2014.

[7] Q. Ziliang, "Three dimensional SAS motion error estimation employing near-field beamforming," *EUSAR 2018: 12th European Conference on Synthetic Aperture Radar, Proceedings of*, pp. 332–337, 2018.

[8] J. Dillon, "Aided Inertial Navigation in GPS-denied Environments Using Synthetic Aperture Processing," DRDC, Tech. Rep. DRDC-RDDC-2016-C200, 2016.

[9] W. A. Connors, A. J. Hunter, and J. Dillon, "Increasing Navigation Effectiveness in GPS Denied Environments Using Through-The-Sensor SAS Techniques," in *4th International Conference on Synthetic Aperture Sonar and Synthetic Aperture Radar 2018*, 2018, pp. 99–106.

[10] P. Rosen, S. Hensley, I. Joughin, F. Li, S. Madsen, E. Rodriguez, and R. Goldstein, "Synthetic aperture radar interferometry," *Proceedings of the IEEE*, vol. 88, no. 3, pp. 333–382, Mar 2000.

[11] T. O. Sæbø, "Seafloor Depth Estimation by means of Interferometric Synthetic Aperture Sonar," PhD Thesis, University of Tromsø, 2010.

[12] D. Billon and F. Fohanno, "Theoretical performance and experimental results for synthetic aperture sonar self-calibration," in *IEEE Oceanic Engineering Society. OCEANS'98. Conference Proceedings*, vol. 2. IEEE, 1998, pp. 965–970.

[13] A. Bellettini and M. Pinto, "Theoretical accuracy of synthetic aperture sonar micronavigation using a displaced phase-center antenna," *IEEE Journal of Oceanic Engineering*, vol. 27, no. 4, pp. 780–789, Oct 2002.

[14] R. S. Raven, "Electronic Stabilization for Displaced Phase Center Systems," U.S. Patent US4 244 036A, Jan. 06, 1981.

[15] R. Sheriff, "Synthetic aperture beamforming with automatic phase compensation for high frequency sonars," in *Proceedings of the 1992 Symposium on Autonomous Underwater Vehicle Technology*, no. 3. IEEE, 1992, pp. 236–245.

[16] D. A. Cook, "Synthetic Aperture Sonar Motion Estimation and Compensation," Master's Thesis, Georgia Institute of Technology, 2007.

[17] R. M. Goldstein, H. A. Zebker, and C. L. Werner, "Satellite radar interferometry: Two-dimensional phase unwrapping," *Radio Science*, vol. 23, no. 4, pp. 713–720, Jul 1988.

[18] M. A. Fischler and R. C. Bolles, "Random sample consensus: a paradigm for model fitting with applications to image analysis and automated cartography," *Communications of the ACM*, vol. 24, no. 6, pp. 381–395, Jun 1981.

[19] P. H. S. Torr and D. W. Murray, "The Development and Comparison of Robust Methods for Estimating the Fundamental Matrix," *International Journal of Computer Vision*, vol. 24, pp. 271–300, 1997.

[20] Haifeng Chen and Meer, "Robust regression with projection based M-estimators," in *Proceedings Ninth IEEE International Conference on Computer Vision*, vol. 2. IEEE, 2003, pp. 878–885.

[21] R. Subbarao and P. Meer, "Beyond RANSAC: User Independent Robust Regression," in *2006 Conference on Computer Vision and Pattern Recognition Workshop (CVPRW'06)*. IEEE, 2006, pp. 101–101.

[22] R. Raguram, O. Chum, M. Pollefeys, J. Matas, and J.-M. Frahm, "USAC: A Universal Framework for Random Sample Consensus," *IEEE Transactions on Pattern Analysis and Machine Intelligence*, vol. 35, no. 8, pp. 2022–2038, Aug 2013.

[23] W. W. J. Bonifant, "Interferometic synthetic aperture sonar processing," PhD thesis, Georgia Institute of Technology, 1999.

[24] R. Heremans, Y. Dupont, and M. Acheroy, "Motion Compensation in High Resolution Synthetic Aperture Sonar (SAS) Images," in *Advances in Sonar Technology*, S. R. Silva, Ed. I-Tech Education and Publishing, Feb 2009, ch. 3, pp. 43–74.

[25] K. Iverson, *A Programming Language*. Wiley, 1962.

[26] P. J. Barclay, "Interferometric Synthetic Aperture Sonar Design and Performance," PhD thesis, University of Canterbury, 2007.

[27] F. Harris, "On the use of windows for harmonic analysis with the discrete Fourier transform," *Proceedings of the IEEE*, vol. 66, no. 1, pp. 51–83, 1978.

[28] G. Franceschetti and R. Lanari, *Synthetic Aperture Radar Processing*. CRC Press, Feb 2018.

Benjamin Thomas Benjamin W. Thomas received the M.Eng. degree in engineering science from the University of Oxford, U.K., in 2015. Currently he is working towards the Ph.D. degree in the field of synthetic aperture sonar with a focus on high-precision navigation estimation and bathymetry estimation using interferometry at the University of Bath, UK. In 2017, he spent three months in La Spezia, Italy as a visiting scientist at the NATO Centre for Maritime Research and Experimentation (CMRE).

Alan Hunter Alan J. Hunter (SM18) received the B.E. (Hons) and Ph.D. degrees in electrical and electronic engineering from the University of Canterbury, Christchurch, New Zealand, in 2001 and 2006, respectively. From 2007 to 2010, he was a Research Associate with the University of Bristol, Bristol, U.K., and from 2010 to 2014, he was a Defense Scientist with TNO (Netherlands Organisation for Applied Scientific Research), The Netherlands. In 2014, he joined the Faculty of Engineering, University of Bath, Bath, U.K., where he is currently a Senior Lecturer. Since 2017, he has been an Adjunct Associate Professor with the Department of Informatics, University of Oslo, Oslo, Norway. His research interests are in underwater acoustics, sonar imaging of the seafloor, and autonomous underwater systems. Dr. Hunter is an Associate Editor of the IEEE JOURNAL OF OCEANIC ENGINEERING.

Samantha Dugelay Dr Samantha Dugelay obtained her PhD in mathematics from the University Paris-Sud, France in 1997. She was sponsored by the French Navy Hydrographic Service (SHOM) and served at IFREMER to exploit deep sea multibeam echo-sounder data for automatic seafloor characterisation. She has since then remained in the maritime domain specialising in high resolution synthetic aperture sonar processing and statistical analysis of high resolution data at University College London and the University of Bath (UK) respectively. She then joined the UK Ministry of Defence where she worked on projects ranging from anti-submarine warfare, autonomy, to sonar simulation for mine countermeasures. After being technical lead at the Defence Science and Technology Laboratory (DSTL) in mine countermeasures, she joined the NATO Science and Technology Centre for Maritime Research and Experimentation (CMRE) in 2013 as a project leader and has been the Program Manager for Autonomous Naval Mine Countermeasures since May 2017. Her main interests lie in synthetic aperture sonar processing, machine learning, autonomy and experimentation at sea with a strong emphasis on operational military relevance.